Energy Proceedings
Vol 47, 2024
ISSN 2004-2965

Design of a Hemispherical Reactor for Solar Thermochemical Cycling with Spectrally-selective Window for Efficiency Enhancement#

Xiaoli Lu[1,2], Jiahui Lou[1,2], Zhenyu Tian[3], Jian Jin[4], Hui Kong[5], Yong Hao[1,2*]

1 Institute of Engineering Thermophysics, Chinese Academy of Sciences, Beijing 100190, PR China

2 University of Chinese Academy of Sciences, Beijing 100049, PR China

3 Key Laboratory of Efficient Utilization of Low and Medium Grade Energy, Tianjin University, Tianjin 300350, PR China

4 School of Environmental Science and Engineering, Huazhong University of Science and Technology, Wuhan 430074, PR China

5 School of Mechanical Engineering, Beijing Institute of Technology, Beijing 100081, PR China

(Corresponding Author: haoyong@iet.cn)

ABSTRACT

Two-step solar thermochemical cycles (STC) for H_2O and CO_2 splitting is a promising technology to produce solar fuel. Reaching up to higher solar-to-fuel efficiencies (e.g., >10%) relies on not only the selection of efficient redox materials, but also devising effective solar reactors. We propose a hemispherical STC reactor design with spectral-selective window for solar flux homogenization and solar collection efficiency enhancement. The new geometry effectively increases the percentage of redox oxide between 1500-1700 °C from 89.8% (for a cylindrical geometry) to 97.6% at 15 kW irradiation. A thermodynamic model is developed, taking into account the geometry, reactions, conservations, spectral selectivity and all the major energy losses. Results show that for a typical ceria-based temperature-swing STC in the range of 900-1600 °C combined with inert gas purging and vacuum pumping, the spectral-selective transmissive coating significantly reduces the re-radiation loss by 69.56%. With solar concentration ratio of 5263, the reactor heating rate increases from 172 °C min^{-1} to 194 °C min^{-1}, decreasing the incident solar energy demand from 703 J g^{-1}_{oxide} to 621 J g^{-1}_{oxide}. More importantly, the solar-to-fuel efficiency increases from 10.58% to 12.14%. Spectral selectivity lowers re-radiation loss (>70%) and effectively maintains high collector efficiency and solar-to-fuel efficiency at low concentration ratios (C<3000).

Keywords: solar thermochemical, carbon dioxide splitting, thermodynamic efficiency analysis

1. INTRODUCTION

It is well known that carbon dioxide emissions from the intensive fossil fuels consumption is one of the main causes of global climate changes. Renewable energy have provided significant support for global green and low-carbon transformation[1], e.g., intermittent solar energy can be converted into stable and high-value solar fuels through thermochemical processes. Two-step thermochemical cycle driven by concentrating solar energy utilizes full-spectrum solar energy to split H_2O/CO_2 into H_2/CO, with high theoretical solar-to-fuel efficiency[2]. Ceria (CeO_2) is a state-of-the-art non-stoichiometric oxide due to its fast redox kinetics and thermochemical cycling stability[3, 4]. The two-step thermochemical cycle of CO_2 splitting based on ceria is expressed as：

Reduction:

$$\mathrm{CeO}_{2-\delta_{\mathrm{red,i}}} \rightarrow \mathrm{CeO}_{2-\delta_{\mathrm{red,f}}} + \frac{\delta_{\mathrm{red,f}} - \delta_{\mathrm{red,i}}}{2}\mathrm{O}_2 \quad (1)$$

Oxidation:

$$\mathrm{CeO}_{2-\delta_{\mathrm{red,f}}} + \left(\delta_{\mathrm{red,f}} - \delta_{\mathrm{red,i}}\right)\mathrm{CO}_2 \rightarrow \mathrm{CeO}_{2-\delta_{\mathrm{red,i}}} + \left(\delta_{\mathrm{red,f}} - \delta_{\mathrm{red,i}}\right)\mathrm{CO} \quad (2)$$

In the reduction step, ceria is reduced from initial oxygen non-stoichiometry $\delta_{red,i}$ to the final oxygen non-stoichiometry $\delta_{red,f}$ at high temperatures (e.g., 1300-1700 °C) and low oxygen partial pressures (typically 10^{-3}-10^{-5} bar). In the oxidation step, the reduced ceria is exposed to an oxidizing gas (CO_2) at low temperatures (e.g., 800-1200 °C) to produce fuel. The key system metric is the solar-to-fuel efficiency $\eta_{solar\text{-}to\text{-}fuel}$[5], defined as the ratio of the high heating value (HHV) of the fuel produced to the solar energy input to the reactor. However, experimental efficiency of CO_2 splitting[6] that has been demonstrated by far is only 5-6%. Therefore, further innovations in reactor design, material development, and operating conditions are necessary to promote efficiency advances.

This is a paper for the 10th Applied Energy Symposium: Low Carbon Cities & Urban Energy Systems (CUE2024), May. 11-12, 2024, Shenzhen, China.

For an ideal solar thermochemical reactor, incident solar energy is primarily employed to drive the reduction reaction. However, energy losses are typically occurred during the practical process, among which re-radiation loss makes up around 9.5-47.6%[6-8] of the incident solar energy. To reduce it, early attempts like the Sandia CR5 reactor with a reverse rotating disk[9]. However, this design was not successfully tested due to poor sealing and mechanical failures[10]. Other concepts include particle gravity-moving countercurrent reactor[11] and radiative recuperator in the particle loop[12], both with significant heat losses (solid heat recovery of less than 50%). Recently, a moving "reactor train system" (RTS) concept (with a theoretical heat recovery efficiency of 80%) has been proposed for radiative heat recovery[13], but practical verification has not been reported. Since rotating/moving reactors encounter significant technical challenges, most current experimental studies focus on fixed-bed types. Non-imaging secondary concentrators[14, 15] and a plano-convex quartz window design[16] have been incorporated with solar receiver aperture of the fixed-bed reactor in order to reduce re-radiation losses and improve collection efficiency.

Besides optical structure optimization mentioned above, the utilization of spectral-selective transmissive coating on the optical window can significantly enhance collection efficiency[17, 18] while maintaining low concentrating ratio[19] (i.e., reducing the complexity and cost of solar concentrating system). The reaction temperature of a thermochemical reactor approximating a blackbody cavity is typically much lower (e.g., 1773 K) than that of the sun (5700 K), so spectrally selective window allows to pass through the majority of incident sunlight while reflecting radiation from the reaction cavity back. Earlier researchers modeled the radiative transfer of a high-temperature solar cylindrical cavity reactor with spectrally selective quartz/sapphire windows[20]. Correlated with thermochemical reaction processes, Jin et al. proposed an efficiency-enhancing design of spectrally selective window of a methane reforming reactor at the temperature of 850 °C, and the simulation results showed that the cutoff wavelength of 2400 nm helped to reduce the re-radiation loss by 80%[21]. Thermodynamic calculations by Hu et al. demonstrated that at a collector temperature of 1000 K, the ideal cutoff wavelength was between 1600 and 2000 nm[22]. Nonetheless, the reduction temperature (1673-1973 K) of two-step thermochemical cycle is higher than those of two reactors mentioned above. By increasing the reduction temperature to 1773 K, Lin et al. achieved a 36.7% relative improvement in solar-to-fuel efficiency at the cutoff wavelength of 1350 nm and concentrating ratio of 1300 [19]. However, specific configuration of STC reactor is not involved in their thermodynamic analysis. Moreover, the application of spectrally-selective coating in the STC reactor requires that it could withstand high temperatures (>500 °C)[6, 23]. Therefore, the thermodynamic feasibility is mainly analyzed in this paper.

Spectrally-selective optical window has the potential to reduce re-radiation loss at low concentration ratios (i.e., reducing concentrator area and cost), which, in combination with optimization of reactor configuration design and operating strategies, could enhance solar-to-fuel efficiency. In this work, an innovative hemispherical thermochemical reactor design with spectrally-selective window for more uniform temperature distribution and enhanced efficiencies is proposed. The enhancement mechanisms of thermal collection efficiency and solar-to-fuel efficiency are investigated, respectively. Sensitive analysis on the window radius and cutoff wavelength at different reduction temperatures is performed.

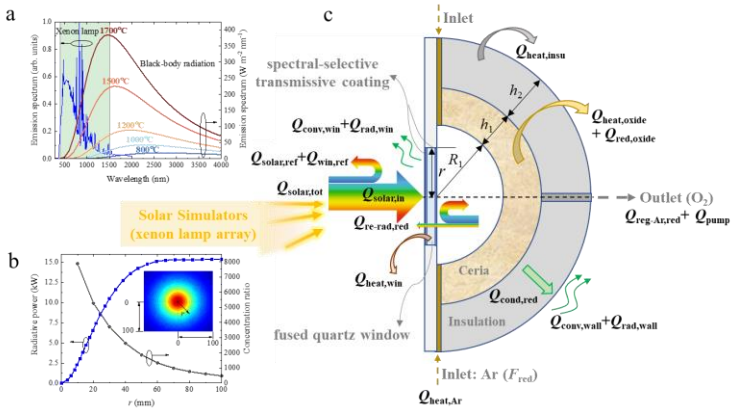

Fig. 1: (a) The emission spectrum of a xenon arc lamp [24] and black-body radiation. (b) Radiative power of xenon lamp array as a function of the radial coordinate from the center of the focal plane [24]. (c) Schematic diagram of a hemispherical solar thermochemical reactor for CO_2 splitting with spectrally-selective window.

2. ANALYTICAL METHODOLOGY

2.1 Modeling of Hemispherical STC Reactor

A conceptual hemispherical solar thermochemical reactor, consisting of fused quartz window (spectrally selective coating on external surface), porous ceria bed and Al_2O_3-SiO_2 insulation layer, is illustrated in Fig 1c. Including the Monte Carlo ray tracing method, a transient model is developed and the operating parameters of the STC reactor are shown in Table1.

Table 1: Operating parameters of the STC reactor

Parameters	Value
Final reduction temperature, $T_{red,f}$	1400~1700 °C
Initial reduction temperature, $T_{red,i}$	900 °C
Total pressure of reduction, $p_{tot,red}$	10^{-3} bar
Flow rate of Ar, F_{red}	0.28 mL min^{-1} g^{-1} [23]
Flow rate of CO_2, F_{ox}	2.80 mL min^{-1} g^{-1} [23]
Radius of quartz window, r	10~100 mm
Inner radius of ceria bed, R_1	80 mm
Thickness of ceria bed, h_1	25 mm
Porosity of ceria bed, ϕ	76% [6]
Thickness of insulation layer, h_2	50 mm

These assumptions are embodied in the model: (1) ceria bed is isotropic with no temperature gradient and concentration gradient; (2) the dynamics of redox material are infinitely rapid to reach a thermodynamic equilibrium (i.e., oxygen partial pressure p_{O_2} at a given oxygen non-stoichiometry $\delta(t)$ equals the oxygen partial pressure of outlet flow)[25]; These ideal conditions allow for the assessment of the upper bound of solar-to-fuel efficiency [26].

The energy balance of the reduction step, shown in Fig 1c, is given as:

$$Q_{solar}(r) = Q_{red,oxide} + Q_{heat,oxide} + Q_{heat,Ar} + Q_{heat,insu} + Q_{wall,loss} + Q_{win,loss} + Q_{re\text{-}rad,red} + Q_{win,ref} \quad (3)$$

where $Q_{red,oxide}$ is the energy required for reducing ceria from δ_{ox} to δ_{red} per unit mass of ceria. The changes of reduction enthalpy and entropy of ceria are taken from literature [27]. n_{oxide} is the molar amount per unit mass of ceria.

$$Q_{red,oxide} = n_{oxide}\int_{\delta_{ox}}^{\delta_{red}} \Delta H(\delta)\,\mathrm{d}\delta \quad (4)$$

$Q_{heat,oxide}$ represents the energy consumption of heating ceria, in which $C_{p,oxide}(T)$ is the specific heat of ceria [7], defined as:

$$Q_{heat,oxide} = n_{oxide}\int_{T_{red,i}}^{T_{red,f}} C_{p,oxide}(T)\,\mathrm{d}T \quad (5)$$

During the reduction step, oxygen partial pressure can be reduced by inert gas (e.g., argon) purging and vacuum pumping to enhance the oxygen non-stoichiometry δ_{red}. The inert gas at a flow rate of F_{red} (mL min^{-1} g^{-1}) is heated to the reduction temperature T_{red} with the specific heat of $C_{p,Ar}(T)$ [7], and this energy consumption is defined as:

$$Q_{heat,Ar} = \int_0^{t_{red}}\int_{T_0}^{T_{red}} F_{red}\cdot C_{p,Ar}(T)\,\mathrm{d}T\mathrm{d}t \quad (6)$$

The ceria bed is wrapped with Al_2O_3-SiO_2 insulation of thickness h_2. $C_{p,insu}(T)$ is the specific heat of Al_2O_3-SiO_2 insulation [7]. n_{insu} is the number of moles of insulation layer used per unit mass of ceria. Energy consumption for heating insulation is given by:

$$Q_{heat,insu} = n_{insu}\int_{T_{red,i}}^{T_{red,f}} C_{p,insu}(T)\,\mathrm{d}\left(\frac{T+T_{wall}}{2}\right) \quad (7)$$

where the temperature T_{wall} of the outer wall of the insulation layer is taken as $T_{wall} = T_{red} - 600$ according to experimental results. The conduction heat loss (dissipated by radiation and convection on the outer wall) of the insulation is calculated per unit mass of ceria with Eq. 8. $\kappa_{insu}(T)$ is the thermal conductivity of Al_2O_3-SiO_2 insulation [7]. Assuming that the inner surface temperature of the insulation layer is the same as that of the ceria bed.

$$Q_{wall,loss} = n_{insu}A_{insu}\int_{T_{red,i}}^{T_{red,f}} \frac{\kappa_{insu}(T)\cdot(T-T_{wall})}{h_{insu}}\mathrm{d}T \quad (8)$$

where the heat transfer area of insulation can be calculated by $A_{insu} = 2\pi\left(R_1 + h_1 + 0.5h_2\right)^2$. $Q_{win,loss}$, energy lost by radiation and convection at the window, amounts to 5% (i.e., heat loss factor f =0.05 [28]) of the energy input through the solar reactor's aperture:

$$Q_{win,loss} = f\cdot Q_{solar,in}(r,\lambda_s) \quad (9)$$

The re-radiation loss $Q_{re\text{-}rad,red}$ is defined as:

$$Q_{re\text{-}rad,red} = \varepsilon_{syn}\pi r^2\int_0^{t_{red}}\int_{300\,nm}^{\lambda_s}\left(\tau_s(\lambda)\cdot\tau_{win}(\lambda)\cdot E_{b,\lambda}(T,\lambda)\right)\mathrm{d}\lambda\mathrm{d}t \quad (10)$$

where ε_{syn} is the apparent emissivity of reaction cavity[7]. λ_s is the cutoff wavelength of spectral-selective transmissive coating; $\tau_{win}(\lambda)$ is the spectral transmittance of pure fused quartz[29]. The spectral transmittance $\tau_s(\lambda)$ of spectral-selective transmissive coating in the wavelength of ($300-\lambda_s$) nm is taken as manufacture's data of 97%[30]. $E_{b\lambda}(T,\lambda)$ is the spectral emission of blackbody according to Planck's law, shown in Fig 1a.

The energy loss $Q_{win,ref}$ reflected and absorbed by the spectral selective window can be calculated by:

$$Q_{win,ref} = Q_{solar}(r) - Q_{solar,in}(r,\lambda_s) \quad (11)$$

where $Q_{solar}(r)$ can be calculated by $Q_{solar}(r) = P_{solar}(r)\times t_{red}$, in which $P_{solar}(r)$ is the radiative power of xenon lamp array[24]. $Q_{solar,in}(r,\lambda_s)$ is the solar energy transmitted through the solar reactor's aperture, determined by:

$$Q_{\text{solar,in}}(r,\lambda_s)=\frac{\int_{300\text{ nm}}^{\lambda_s\text{ nm}}\tau_s(\lambda)\cdot\tau_{\text{win}}(\lambda)\cdot E_{\text{Xe},\lambda}(\lambda)\,\mathrm{d}\lambda}{\int_{300\text{ nm}}^{4000\text{ nm}}E_{\text{Xe},\lambda}(\lambda)\,\mathrm{d}\lambda}\times Q_{\text{solar}}(r) \quad (12)$$

where $E_{\text{Xe},\lambda}(\lambda)$ is the emission spectrum of a xenon arc lamp [24] shown in Fig 1a. $Q_{\text{solar,ref}}$ indicates the solar energy loss reflected by the front surface of the STC reactor (i.e., beyond the optical window), calculated by:

$$Q_{\text{solar,ref}}=Q_{\text{solar,tot}}-Q_{\text{solar}}(r) \quad (13)$$

where $Q_{\text{solar,tot}}=P_{\text{solar,tot}}\times t_{\text{red}}$ ($P_{\text{solar,tot}}$ is the total radiative power of the xenon lamp array at an aperture radius of 100 mm)[24].

2.1.1 Thermal Collection Efficiency

The thermal collection efficiency $\eta_{\text{abs,i}}$ of the hemispherical STC reactor is defined as follows:

$$\eta_{\text{abs,i}}=\frac{Q_{\text{solar,abs}}}{Q_{\text{solar,tot}}}=\frac{Q_{\text{solar,tot}}-Q_{\text{solar,loss}}}{Q_{\text{solar,tot}}}\times 100\% \quad (14)$$

where the total energy loss $Q_{\text{solar,loss}}$ can be defined by the following relationship:

$$Q_{\text{solar,loss}}=Q_{\text{re-rad,red}}+\left(Q_{\text{win,ref}}+Q_{\text{solar,ref}}\right)+Q_{\text{win,loss}}+Q_{\text{wall,loss}} \quad (15)$$

$\eta_{\text{abs,1}}$ and $\eta_{\text{abs,2}}$ represent the thermal collection efficiencies of the STC reactor without/with spectral-selective coating, respectively.

2.1.2 Solar-to-fuel Efficiency

The solar-to-fuel efficiency ($\eta_{\text{solar-to-fuel}}$) is defined by Eq. 16, in which n_{CO} (in mol) is the cumulative productivity of carbon monoxide per unit mass of ceria per cycle. The calculation of the production rates of oxygen and fuel is based on the thermo-kinetic model established by Davenport et al. [25]. HHV_{CO} is the molar heating value of CO (283 kJ mol^{-1}):

$$\eta_{\text{solar-to-fuel}}=\frac{n_{\text{CO}}\cdot\text{HHV}_{\text{CO}}}{Q_{\text{solar}}(r)+Q_{\text{reg-Ar,red}}+Q_{\text{pump}}} \quad (16)$$

where $Q_{\text{reg-Ar,red}}$ and Q_{pump} are the energy consumptions for argon regeneration and vacuum pumping during the reduction step, referenced from Marxer's article[6].

3. RESULTS AND DISCUSSION

3.1 Temperature Uniformity in STC Reactors

Compared with a typical cylindrical reactor (with same inner radius R_1 and thickness h_1), the hemispherical reactor exhibits more homogeneous temperature distribution. For example, at a heating time t=300 s, more than 90% of the volume of ceria in these two types of reactors is heated to over 1500 °C, and the volume fractions between 1500-1700 °C (T > 1700 °C, at risk of superheated sublimation; T < 1500 °C, insufficiently reduced) are 89.8% (cylindrical) and 97.6%, respectively. According to the temperature distributions in Fig 2a and Fig 2b, there is an obvious localized over-shoot of temperature in the central region at the bottom of the cylindrical ceria bed. As for the hemispherical ceria bed, the uniformity of irradiation on the light-facing surface is improved due to the approximately equidistant reception of the rays emitted from the focal point, which in turn demonstrates a more uniform temperature distribution.

3.2 Effect of Spectral Selectivity on Hemispherical STC Reactor

3.2.1 Analysis of Thermal Collection Efficiency

For the case without spectral-selective transmissive coating on the optical window, concentrating light passes through the quartz window and heats the ceria bed, while the re-radiation loss escapes through the optical aperture. The thermal collection efficiency $\eta_{\text{abs,1}}$ is defined by Eq. 14. According to Fig 3a, under the condition of the same window radius r, the collector efficiency is decreased due to the significant loss of re-radiation at high temperatures. The optimum thermal collector efficiency $\eta_{\text{abs,1-opt}}$ (73.59%) in the selected parameter combinations occurs at $r_{\text{opt,1}}$=50mm and $T_{\text{red,f}}$ =1500 °C. The reason can be derived from the distribution of energy consumption (Fig 3b) that expanding window radius leads to a predominance of re-

a

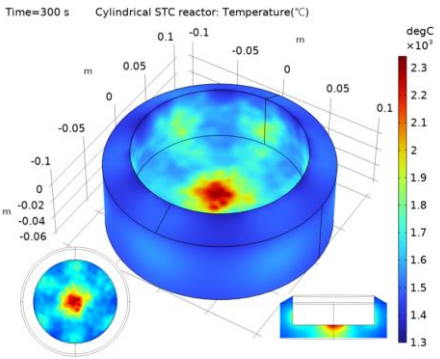

b

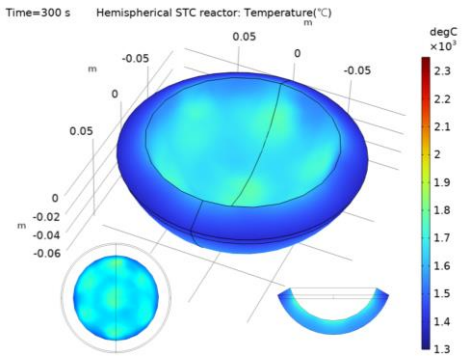

Fig. 2: Temperature distribution (t=300s) of ceria bed in (a) cylindrical and (b) hemispherical STC reactors.

radiation loss, whereas reducing it results in insufficient incident radiation power $P_{solar}(r)$ (i.e., longer heating time).

For the case of quartz window with spectral-selective coating, Fig 3c depicts the enhancement of the collector efficiency of hemispherical STC reactor at $T_{red,f}$ =1500 °C. The optimum collector efficiency $\eta_{abs,2\text{-}opt}$ (81.78%) occurs at window radius $r_{opt,2}$=60 mm (vs. $r_{opt,1}$=50 mm) and cutoff wavelength $\lambda_{s\text{-}opt}$ =1600 nm. Fig 3b and 3d provides a detailed comparison of solar energy utilization for these two points of optimal collector efficiency. Although the spectrally selective coating increases the energy loss of window reflection ($Q_{win,ref}$ / $Q_{solar,tot}$) from 4.62% to 8.40%, it simultaneously reduces the re-radiation loss ($Q_{re\text{-}rad}$ / $Q_{solar,tot}$) from 11.92% to 3.78% and increases the incident radiation power $P_{solar}(r)$ due to enlarged optical aperture (i.e., $Q_{solar,ref}$ / $Q_{solar,tot}$ is reduced from 5.42% to 1.04%). The heating time is shortened from 1.49 min to 1.24 min (i.e., reducing total solar energy input $Q_{solar,tot}$ within a 100 mm radius by 16.75%), which ultimately results in a relative enhancement in the reactor's thermal collection efficiency by about 11.13%.

3.2.2 Analysis of STC Cycling Performance

The effect of spectral selectivity on the hemispherical STC reactor's thermochemical performance is discussed. Under the condition of $T_{red,f}$ = 1500 °C, $T_{red,i}$ = 900 °C and r = 60 mm, the total energy consumption (i.e., the denominator of the solar-to-fuel efficiency $\eta_{solar\text{-}to\text{-}fuel}$) is reduced from 599 J g^{-1}_{oxide} to 485 J g^{-1}_{oxide} through spectral selectivity, so that $\eta_{solar\text{-}to\text{-}fuel}$ is increased from 5.01% to 7.81%. Increasing the final reduction temperature $T_{red,f}$, the enhancement in solar-to-fuel efficiency is more pronounced due to shorter heating time. By comparing the results of the final reduction temperatures $T_{red,f}$ = 1500 °C and $T_{red,f}$ = 1700 °C, the re-radiation losses are reduced by 82.55% and 81.56%, respectively. The total energy consumptions are reduced by 19.13% ($T_{red,f}$ = 1500 °C) and 29.88% ($T_{red,f}$ = 1700 °C), respectively, due to the shortening of the heating time by nearly 0.3 min and 1 min, which reduces the time-dependent energy consumptions (e.g., gas-phase sensible heat, energy consumptions of pumping and argon regeneration and, radiation and convection losses from spectrally-selective window and the outer wall of hemispherical STC reactor). Finally, the solar-to-fuel efficiencies are enhanced from 5.01% to 7.81% ($T_{red,f}$ = 1500 °C) and 9.58% to 14.63% ($T_{red,f}$ = 1700 °C), respectively.

Fig 4 shows the sensitive analysis of cut-off wavelength λ_s and window radius r. Under the final reduction temperature $T_{red,f}$ = 1500 °C, the optimal solar-to-fuel efficiency $\eta_{solar\text{-}to\text{-}fuel}$ is 8.20% (λ_s=1900 nm and

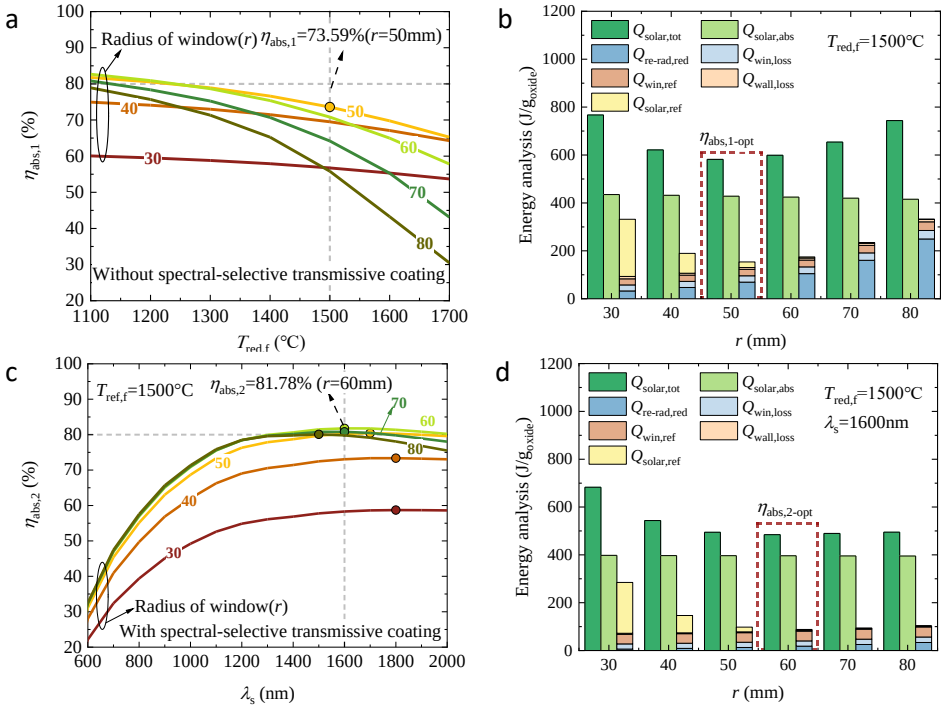

Fig. 3: Thermal collection efficiency of the hemispherical STC reactor without (a) or with (c) spectral-selective transmissive coating. The efficiency $\eta_{abs,1}$ (a) is a function of the final reduction temperature $T_{red,f}$ and the radius of quartz window r, and the efficiency $\eta_{abs,2}$ (c) is a function of the cutoff wavelength λ_s and the radius of quartz window r. Energy analysis for the hemispherical STC reactor with (b) or without (d) spectral selectivity under $T_{red,f}$ =1500°C.

r=20 mm). Although the small window radius reduces the incident radiative power (15.08 kW and 6.61 kW for r=60 mm and r=20 mm, respectively), resulting in longer heating time (1.24 min for point B_1, 3.60 min for point A_1, shown in Fig 4), it significantly reduces the re-radiation losses. Therefore, the solar-to-fuel efficiency $\eta_{solar\text{-}to\text{-}fuel}$ is enhanced by the reduction in total energy consumption. However, for a solar concentrating system with given optical characteristic, small optical window results in significant increase of energy losses ($Q_{solar,ref}$) reflected by the front surface of the reactor, which mainly leads to the decrease in the thermal collector efficiency from 81.78% (r=60 mm of point B_1) to 36.09% (r=20 mm of point A_1), respectively. Expanding window radius (r≥40 mm), spectral selectivity lowers re-radiation loss (>70%) and effectively maintains high collector efficiency and solar-to-fuel efficiency at low concentration ratios (C<3000), which is more applicable for outdoor solar concentrators.

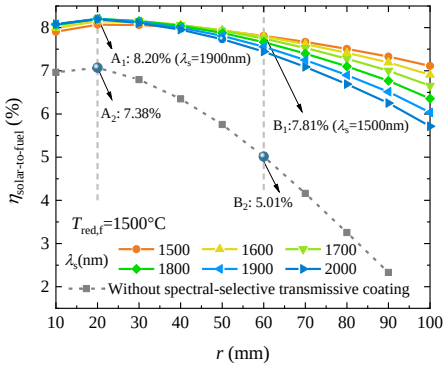

Fig. 4: Effect of cutoff wavelength and radius on solar-to-fuel efficiency.

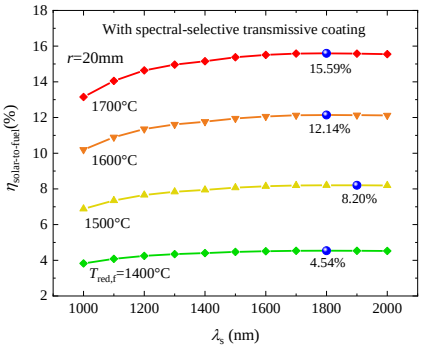

Fig. 5: Sensitivity analysis of optimal cutoff wavelength with respect to final reduction temperature.

The solar-to-fuel efficiency can be significantly enhanced from 10.58% to 12.14% under the conditions of $T_{red,f}$=1600 °C, r=20mm (C=5263), and λ_s=1800 nm. The re-radiation loss is reduced by 69.56% and the heating rate is increased from 172 °C min^{-1} to 194 °C min^{-1} (i.e., the period of reduction reaction is shortened from 4.07 min to 3.60 min). Therefore, the total solar energy input per unit mass of ceria is reduced from 703 J g$^{-1}_{oxide}$ to 621 J g$^{-1}_{oxide}$. Comparison among the efficiency curves (Fig 5) corresponding to different temperatures shows that λ_s=1800~1900 nm is optimal for the cases of r=20 mm (similar results of r=60mm).

This work aims to explore the mechanisms of the effect of spectral selectivity on the two efficiencies through in-depth energy analysis correlated with the practical STC reactor operating process. For practical applications, further analysis of coating preparation process, high temperature durability, cost and other factors is required.

4. CONCLUSION

A novel hemispherical thermochemical reactor with spectrally-selective window design for efficiency enhancement is proposed. The following could be concluded:

（1） Compared with conventional cylindrical STC reactor, the hemispherical geometry delivers more homogeneous temperature distribution within the ceria bed, reducing the temperature difference from 450 °C to 200 °C; the volume fraction of over-temperature above 1700°C is significantly reduced from 9.07% to 2.14%, resulting in improved temperature uniformity.

（2） At the final reduction temperature of 1600 °C, the solar-to-fuel efficiency $\eta_{solar\text{-}to\text{-}fuel}$ can be enhanced from 10.58% to 12.14% (r = 20 mm, λ_s = 1800 nm, C=5263) due to the substantial increase in the heating rate of the STC reactor by 12.8%, and the reduction in the total solar energy consumption by 15.94%.

（3） Spectral selectivity lowers re-radiation loss (>70%) and effectively maintains collector efficiency and solar-to-fuel efficiency at low concentration ratios (C<3000).

5. ACKNOWLEDGEMENTS

This work is supported by the Basic Science Center Program for Ordered Energy Conversion of the National Natural Science Foundation of China (No. 52488201).

REFERENCES

[1] Budama V K, Duarte J P R, Roeb M, et al. Potential of solar thermochemical water-splitting cycles: A review [J]. Solar Energy, 2023, 249: 353-366.

[2] Song H, Luo S Q, Huang H M, et al. Solar-Driven Hydrogen Production: Recent Advances, Challenges, and Future Perspectives [J]. ACS Energy Letters, 2022, 7(3): 1043-1065.

[3] Zoller S, Koepf E, Nizamian D, et al. A solar tower fuel plant for the thermochemical production of kerosene from H_2O and CO_2 [J]. Joule, 2022, 6(7): 1606-1616.

[4] Lu Y, Zhu L, Agrafiotis C, et al. Solar fuels production: Two-step thermochemical cycles with cerium-based oxides [J]. Progress in Energy and Combustion Science, 2019, 75: 100785.
[5] Steinfeld A. Solar thermochemical production of hydrogen—a review [J]. Solar Energy, 2005, 78(5): 603-615.
[6] Marxer D, Furler P, Takacs M, et al. Solar thermochemical splitting of CO_2 into separate streams of CO and O_2 with high selectivity, stability, conversion, and efficiency [J]. Energy & Environmental Science, 2017, 10(5): 1142-1149.
[7] Zoller S, Koepf E, Roos P, et al. Heat Transfer Model of a 50 kW Solar Receiver–Reactor for Thermochemical Redox Cycling Using Cerium Dioxide [J]. Journal of Solar Energy Engineering, 2019, 141(2): 021014.
[8] Furler P, Steinfeld A. Heat transfer and fluid flow analysis of a 4kW solar thermochemical reactor for ceria redox cycling [J]. Chemical Engineering Science, 2015, 137: 373-383.
[9] Yuan C S, Jarrett C, Chueh W, et al. A new solar fuels reactor concept based on a liquid metal heat transfer fluid: Reactor design and efficiency estimation [J]. Solar Energy, 2015, 122: 547-561.
[10] Diver R B, Miller J E, Siegel N P, et al. Testing of a CR5 Solar Thermochemical Heat Engine Prototype [M]. 2010: 97-104.
[11] Ermanoski I, Siegel N P, Stechel E B. A New Reactor Concept for Efficient Solar-Thermochemical Fuel Production [J]. Journal Of Solar Energy Engineering-transactions Of The Asme, 2013, 135(3): 031002.
[12] Budama V K, Johnson N G, McDaniel A, et al. Thermodynamic development and design of a concentrating solar thermochemical water-splitting process for co-production of hydrogen and electricity [J]. International Journal of Hydrogen Energy, 2018, 43(37): 17574-17587.
[13] Patankar A S, Wu X Y, Choi W, et al. A Reactor Train System for Efficient Solar Thermochemical Fuel Production [J]. Journal Of Solar Energy Engineering-transactions Of The Asme, 2022, 144(6): 061014.
[14] Romero M, Steinfeld A. Concentrating solar thermal power and thermochemical fuels [J]. Energy & Environmental Science, 2012, 5(11): 9234-9245.
[15] Chueh W C, Falter C, Abbott M, et al. High-Flux Solar-Driven Thermochemical Dissociation of CO_2 and H_2O Using Nonstoichiometric Ceria [J]. Science, 2010, 330(6012): 1797-1801.
[16] Shuai Y, Wang F Q, Xia X L, et al. Radiative properties of a solar cavity receiver/reactor with quartz window [J]. International Journal of Hydrogen Energy, 2011, 36(19): 12148-12158.
[17] Gao Y, Wang Z, Ding D, et al. Novel Methods to Harness Solar Radiation for Advanced Energy Applications [J]. ES Energy & Environment, 2019, 5: 1-7.
[18] Zhang B W, Li L, Chamoli S K, et al. Design of near-ideal and omnidirectional selective solar absorber for high-temperature applications [J]. Solar Energy Materials and Solar Cells, 2023, 257: 112383.
[19] Lin P, Lou J, Li J, et al. Effect of spectral-selectivity on the performance of thermochemical cycling driven by concentrated solar energy [J]. Journal of Tsinghua University Science and Technology, 2021, 61(12): 1389-1396.
[20] Maag G, Falter C, Steinfeld A. Temperature of a Quartz/Sapphire Window in a Solar Cavity-Receiver [J]. Journal Of Solar Energy Engineering-transactions Of The Asme, 2011, 133(1): 014501.
[21] Jin J, Wei X, Liu M K, et al. A solar methane reforming reactor design with enhanced efficiency [J]. Applied Energy, 2018, 226: 797-807.
[22] Hu P, Liu Y, Zhang Q, et al. Thermodynamic analysis on medium-high temperature solar thermal systems with selective coatings [J]. Science China-Technological Sciences, 2013, 56(12): 3137-3143.
[23] Zoller S. A 50 kW solar thermochemical reactor for syngas production utilizing porous ceria structures [D], 2020.
[24] Bader R, Haussener S, Lipinski W. Optical Design of Multisource High-Flux Solar Simulators [J]. Journal Of Solar Energy Engineering-transactions Of The Asme, 2015, 137(2): 021012.
[25] Davenport T C, Yang C K, Kucharczyk C J, et al. Implications of Exceptional Material Kinetics on Thermochemical Fuel Production Rates [J]. Energy Technology, 2016, 4(6): 764-770.
[26] Jarrett C, Chueh W, Yuan C, et al. Critical limitations on the efficiency of two-step thermochemical cycles [J]. Solar Energy, 2016, 123: 57-73.
[27] Panlener R J, Blumenthal R N, Garnier J E. A thermodynamic study of nonstoichiometric cerium dioxide [J]. Journal of Physics and Chemistry of Solids, 1975, 36(11): 1213-1222.
[28] Charvin P, Stephane A, Florent L, et al. Analysis of solar chemical processes for hydrogen production from water splitting thermochemical cycles [J]. Energy Conversion and Management, 2008, 49(6): 1547-1556.
[29] Ideal Vacuum Products L. https://www.idealvac.com/files/manuals/IVP-Viewing-Window-Manual-V1.3.0.pdf [M]. 2018.
[30] Schneider-Kreuznach. https://schneiderkreuznach.com/application/files/6316/8785/4432/Schneider-Kreuznach_Datasheet_Shortpass_SP_850_2023.pdf [M]. 2023.